MAE 6755 Finite Element Method: Theory and Applications in Mechanics and Multiphysics

Project 1

Cavity failure in homogeneous and fractured media

Under the guidance of :
Prof. Chloe Arson
Dr Alec Tristani

By:
Somesh Pratap Singh

Contents

1 Problem Statement

A circular tunnel of diameter 2a = 10 meters and located at a depth of 100 m is subjected to a biaxial state of stress, as illustrated in the figure1.

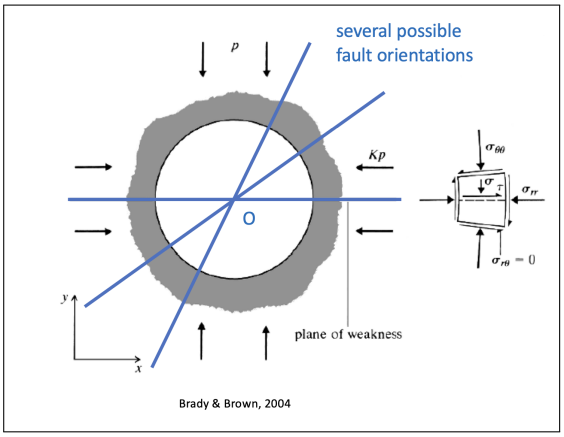

Figure 1 Problem Statement

A fault plane intersects the tunnel cross section, passing through the centroid O of the section. We aim to study various fault orientations, several stresses p and K*p, and several rock mass properties. The goal of this project is to examine in which conditions the rock mass yields in tension or in shear.

2 Step1a: Modeling the cavity in base case without any fault

Given the specefic weight is of the order 2500 kg/m^3. We model the free cavity without fault, for different values of K with the FEM.

2.1 Model Setup

2.1.1 Geometry

The model domain is a square region of size 100×100 meters, with a circular tunnel of radius $a = 5$ meters at the center. The coordinates for the tunnel boundary and domain corners are defined in the '.geo' file using Gmsh. The tunnel is centered at the origin $(0, 0)$. The outer square domain is defined from $-L$ to L in both x and y directions, where $L = 50$ m. Figure2 below shows the meshed 2D surface of the domain.

2.1.2 Material Constitutive Models and Parameters

We use a linear elastic isotropic model to represent the behavior of granite. The constitutive model is implemented using the 'ComputeIsotropicElasticityTensor' module. The material parameters used are:

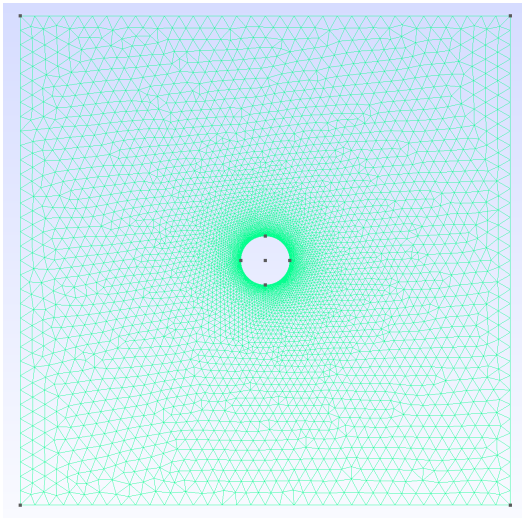

Figure 2 Geometry used for simulating tunnel. The .geo file for this is provided in the code with the name `tunnel_refined.geo`.

- Young's modulus: $E = 52$ GPa
- Poisson's ratio: $\nu = 0.25$

The stress-strain relationship is taken to be Hooke's law for small strains. Additionally, an eigenstrain formulation is used to incorporate the initial in-situ stresses.

2.1.3 Boundary and Initial Conditions

We apply initial stress conditions of in-situ ground stresses before starting. The vertical stress is calculated as:

$$\sigma_v = \gamma g h = 2500 \times 10 \times 100 = 2.5 \times 10^6 \text{ Pa} = s_0$$

where γ is the specific weight of rock, g is the gravitational acceleration, and h is the depth. The horizontal stress is calculated as:

$$\sigma_h = K \cdot s_0$$

Boundary conditions are applied as follows:

- Vertical pressure: s_0 on the top and bottom boundaries.
- Horizontal pressure: σ_h on the left and right boundaries.
- This is done using 'Pressure' boundary conditions in the MOOSE input file.

2.1.4 Mesh Density

We generate mesh using Gmsh with two characteristic lengths to control mesh resolution:

- Near the tunnel: $cl1 = 0.1$ m for refined mesh.
- Far from the tunnel: $cl2 = 3.0$ m for coarser mesh.

This is done to ensure higher resolution near the tunnel to account for stress concentration as this seems a susceptible.

2.1.5 Interpolation

The displacement variables `disp_x` and `disp_y` are interpolated using first-order Lagrange finite elements. The finite element basis functions are specified using the following lines in the MOOOSE input file:

```
order = FIRST
family = LAGRANGE
```

2.1.6 Solver and Modules Used in MOOSE

The simulation is conducted using the 'Steady' executioner with a Newton-Raphson iterative solver. In the present simulations, the PETSc linear solver is used to solve the linear systems. To ensure robustness and numerical stability—especially in the presence of discontinuities like faults, direct solver strategy is adopted. The LU (Lower-Upper) factorization method is used within PETSc (Portable, Extensible Toolkit for Scientific Computation, it is a toolkit developed by Argonne National Labs).

LU factorization decomposes the system matrix into a product of lower and upper triangular matrices. This is useful in quasi-static simulations and avoids the convergence issues.

```
solve_type = NEWTON
petsc_options_iname = '-pc_type'
petsc_options_value = 'lu'
```

The key physics module used is 'SolidMechanics/QuasiStatic' configured for small strain analysis. The stress outputs include both principal and von Mises stress components.

The following MOOSE modules and kernels are employed:

- `ComputeIsotropicElasticityTensor`
- `ComputeLinearElasticStress`
- `ComputeEigenstrainFromInitialStress`
- `QuasiStatic` for time-independent analysis

2.2 Results

To analyze the stress distribution around a free cavity under different stress ratios, we simulate the model for several values of the horizontal-to-vertical stress ratio, $K = \sigma_h/\sigma_v$. The specific weight of rock is taken as $2500\,\mathrm{kg/m^3}$ and depth $h = 100\,\mathrm{m}$, resulting in a vertical stress of $s_0 = \gamma g h = 2.5 \times 10^6\,\mathrm{Pa}$.

The following cases were simulated:

- **Case 1:** $K = 0.25$

- **Case 2:** $K = 0.5$
- **Case 3:** $K = 1.0$
- **Case 4:** $K = 2.0$

In each simulation, the stress components σ_{xx}, σ_{yy}, σ_{xy} and displacements u_x, u_y were recorded along a horizontal line just outside the tunnel boundary (starting at $x = 5.2$ m) extending toward the right boundary (i.e. till $x = 49.5$ m, just before the edge).

We then transform the stresses in the $x - y$ coordinates to $r - \theta$ coordinates. This is done in the python code file names kirsch.py attached with the submission. After we have σ_{rr}, $\sigma_{r\theta}$, $\sigma_{\theta\theta}$, we plot both the analytical solution from the kirsch equation and our results from the simulation on the same graph. r varying from 5.2 to 49.5.

Comparison with Kirsch Equations

The Kirsch solution provides an analytical expression for stress around a circular hole in an infinite, elastic, and isotropic medium under far-field biaxial stress. The analytical solutions predict:

$$\sigma_{\theta\theta}(a, \theta) = \sigma_h + \sigma_v - 2(\sigma_h - \sigma_v)\cos(2\theta)$$

$$\sigma_{rr}(a, \theta) = 0$$

$$\sigma_{r\theta}(a, \theta) = -(\sigma_h - \sigma_v)\sin(2\theta)$$

The FEM simulation results align closely with these predictions. Figure3 shows stress components σ_{xx} and σ_{yy} along the horizontal line, for different K values. All the five plots for different K values can be found in the project submission directory at $\sim$/1a/1afigs. The individual images have gotten a bit too small here but they do indicate the close agreement.

For $K = 1.0$, the stress distribution around the cavity almost becomes symmetric, as predicted. When $K \neq 1$, we observe anisotropy and a shift in the maximum hoop stress direction, which is also consistent with analytical solution.

All the data through which the plots were made can also be obtained at $\sim$/1a/1adata.

2.3 Interpretations

Physical Behavior

The simulation tell us that the stress concentration around the tunnel depends ratio K. For lower values of K (e.g., 0.25) vertical stresses dominate, this leads to higher compressive stress concentrations on the crown $r = a$. Higher K values (e.g., 1.5) show opposite of this behaviour, having dominant horizontal stress concentrations.

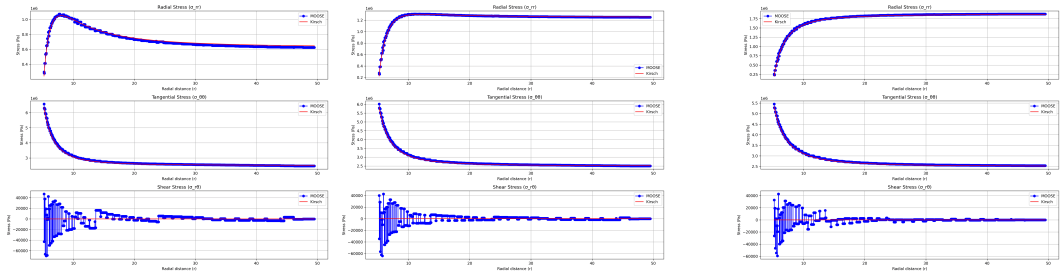

(a) K = 0.25 **(b)** K = 0.5 **(c)** K = 0.75

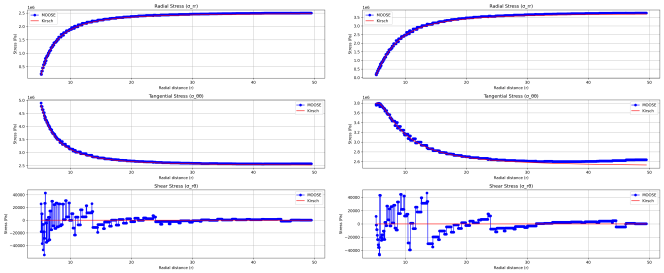

(d) K = 1.0 **(e)** K = 1.5

Figure 3 Stress distribution comparison for different K values between MOOSE simulation results and analytical Kirsch equations. We observe a good agreement.

Table 1 Mean Relative Error (in %) between the Kirsch Solution and the Simulation Results from MOOSE.

Values of K	$K = 0.25$	$K = 0.5$	$K = 0.75$	$K = 1$	$K = 1.5$
σ_{rr}	0.7	0.2	0.5	1.05	2.14
$\sigma_{\theta\theta}$	1.33	1.01	0.97	1.1	1.48
$\sigma_{r\theta}$	0.25	0.18	0.12	0.16	0.31

Accuracy and Error Analysis

The simulation results show good agreement with the analytical Kirsch solutions with the general trend of error increasing around the low K and high K values. Table1 shows the values of mean relative error (in %) for different values of K.

Deviations are observed far from center. This might be due to:

- Finite domain size (Kirsch assumes infinite domain size)
- Discretization error in FEM (at mesh transitions)
- Simplified boundary condition implementation

Computation Cost and Stability

All the simulations were run MacOS M1 chip and the computation time was not bad for any of the cases, generally simulations completed within two minutes. LU decomposition was of help here for solver stability and convergence. The Newton-Raphson scheme helped due to the linear elastic nature of the problem. The results for sampled for 1000 points on the horizontal line. This was then used for post-processing.

3 Step 1b: Modeling the cavity in base case without any fault for three different rock types

The three rocks we choose for analysis in this section are Granite, Fine-grained Sandstone, Muddy Siltstone and do the same steps and analysis as is done in the above section. Model setup and geometry for this section is exactly the same as the one in the above section except the material properties which are shown in Table2. These values are taken from the references which are put at the end of this section. Values for Granite were quite standard throughout the internet and were taken from a credible website www.engineeringtoolbox.com. The values for other two rock types were taken from a research paper on rock studies from Ordos Basin, China. The references are at the end of this section.

3.1 Rock Properties

The properties for three rock types are listed below. Shear strength τ_{max} is computed from the Mohr-Coulomb criterion:

$$\tau_{\text{max}} = c + \sigma_n \tan \phi \tag{1}$$

Where c is cohesion and ϕ is the friction angle. Normal stress σ_n is taken as $p * K$.

Table 2 Mechanical properties of rocks used in simulation

Rock	γ [kg/m^3]	E [GPa]	ν	Tensile Strength [MPa]	Cohesion [MPa]	ϕ [°]
Granite	2700	52.0	0.25	5.27	27.0	55.0
Sandstone	2543	26.26	0.246	6.43	28.6	45.7
Siltstone	2597	23.3	0.198	4.08	25.075	38.06

3.2 Results and Interpretations

For each rock, we did the simulation at $K = 1.0$ and $K = 0.5$. For all cases, radial (σ_{rr}), tangential ($\sigma_{\theta\theta}$), and shear ($\sigma_{r\theta}$) stress distributions were plotted.

Mohr's circles were constructed at selected angular positions ($\theta = 15°$, $30°$, $45°$, $60°$, $75°$, $90°$) along the cavity wall. The code and methodology is present in the file:

~/1b/1bcodes/shear_check.py

The simulation results for the three rock types are presented below.

- **Granite:** Stresses near the cavity were way above than the prescribed Tensile strength for the case $K = 0.5$ and it was just near the Tensile strength for the case, $K = 1$. From the Mohr circle calculations, shear stresses remained below the computed shear strength for all the angles taken into account.
- **Sandstone:** Stresses near the cavity were close to Tensile strength but not exceeding for the case $K = 0.5$ and it was well below the Tensile strength for the case $K = 1$. Shear stresses remained below the computed shear strength for all the angles taken into account.

- **Siltstone:** For both the values of K, stresses near the cavity were way above its Tensile strength. Shear stresses remained below the computed shear strength for all the angles taken into account.

Representative images for Siltstone for the tensile case and shear case $K = 1$ and $K = 0.5$ are shown below Figure4. A total of 12 plots 2 (K) values x 2 plots for each rock (tensile and shear) x 3 rock types are present in the directoty $\sim /1b/1bfigs/rock\_type$.

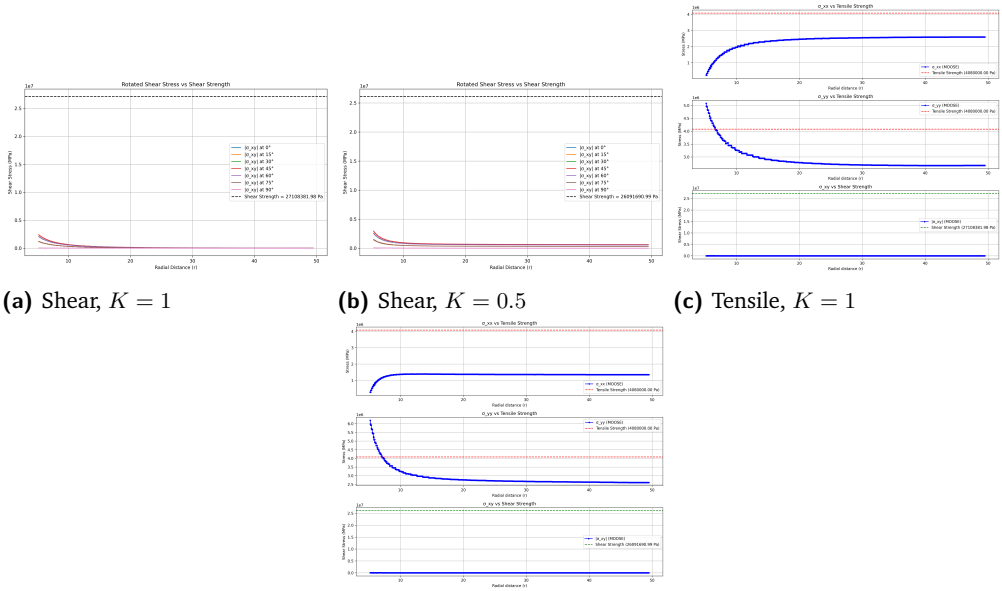

(a) Shear, $K = 1$ **(b)** Shear, $K = 0.5$ **(c)** Tensile, $K = 1$

(d) Shear, $K = 0.5$

Figure 4 Results of simulations performed for Siltstone for various stress conditions.

We had some deviation/noise for shear stress ($\sigma_{r\theta}$), likely due to mesh discretization or numerical interpolation near stress singularities.

Computation cost and Stability: Almost all the simulations for three rock types converged and were completed within two minutes.

3.3 Soruces used for properties of three types of rocks used in the analysis

1. `https://www.engineeringtoolbox.com/young-modulus-d_417.html`
2. Study on the rock physical mechanical properties evaluation of tight oil reservoir in Chang 7 member, Longdong area, Ordos Basin, China.
3. `https://www.engineeringtoolbox.com/poissons-ratio-d_1224.html`
4. Hampton, J., Frash, L., Matzar, L., & Gutierrez, M. (2018). Extended-term monitoring of acoustic emissions post-laboratory hydraulic fracturing. ARMA US Rock Mechanics Symposium.

4 Step2: One Vertical Fault

4.1 Model Setup

4.1.1 Geometry and Mesh

We choose granite for this case. We use 2D plane strain model, simulating a vertical cross-section with a vertical fault. The geometry extends 100 m vertically and horizontally ($x \in [-50, 50]$, $y \in [-50, 50]$). The circular tunnel has a radius of 5 m, centered at the origin. The vertical fault is located along $x = 0$, domain split into left and right rock domains. The mesh for the vertical fault is shown in Figure5. Meshing was done using Gmsh. Same mesh

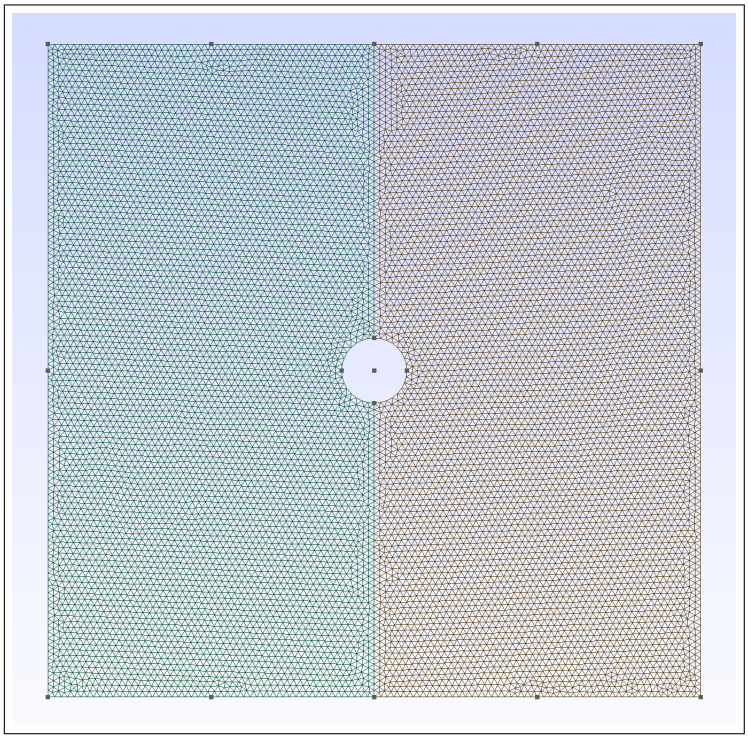

Figure 5 Mesh for the vertical fault case. Geometry file created using gmsh and meshed using the same tool.

resolution was used throughout both the domains unlike in the previous case where we used finer resolutions near the tunnel surface. Quadratic interpolation was used through MOOSE's default Lagrange shape functions of order FIRST.

4.1.2 Material Model and Parameters

The rock material used is granite, modeled as linear elastic. The material properties are:

- Young's Modulus: $E = 52 \times 10^9$ Pa
- Poisson's Ratio: $\nu = 0.25$

Initial stress conditions are applied using the `ComputeEigenstrainFromInitialStress` module and modeled as pressure.

4.1.3 Fault Modeling

The vertical fault is implemented using MOOSE's `Contact` module with the following properties:

- Contact model: Coulomb friction
- Friction coefficient: 0.3
- Formulation: Penalty method with a penalty of 8×10^9 Pa
- Hard normal contact (non-penetrability) and frictional tangential slip

4.1.4 Boundary and Initial Conditions

- Vertical stress applied on top and bottom boundaries based on $s_0 = -\rho g H$, H being the depth.
- Horizontal stress on the left boundary as $\sigma_h = K s_0$.
- Dirichlet BCs used to fix displacement on top, bottom, left, right boundaries.

4.1.5 Solver and Modules

- Executioner: `Steady`, nonlinear solver: Newton-Raphson with no line search
- Solid mechanics module in small strain mode
- Output: CSV and Exodus formats; LineValueSampler used for postprocessing

4.2 Results

4.2.1 Simulation Cases

We analyse the case for various values of p which is handled through varying depth and various values of K. We design a full factorial experiment for values 3 values for K and 3 values for depth. This results in a total of 9 experiments.

- Depth $H = \{50, 80, 100\}$ m
- Stress ratio $K = \{0.5, 1.0, 1.5\}$

For each case, the shear stress τ_{xy} were extracted along radial lines at angles $\theta = 0°, 15°, 30°, 45°, 60°, 90°$ and normal stress along the line y = 0 using `LineValueSampler`.

4.2.2 Plots and Visualizations

For each of the nine cases, Table3 mentions whether the stresses exceed the Tensile strength or Shear Strength in any of Tension or in Shear.

Figure6 shows the normal and shear stresses plotted for various depths, for $K = 1$. Plots for all the nine experiments (total of 18 plots 1 each for tensile and shear) can be found in $\sim /2\_v\_fault/k\_value/depth\_value$.

Depth (m)	K = 0.5	K = 1.0	K = 1.5
50	No	Yes (38)	Yes (41)
80	Yes (48)	Yes (36)	Yes (33)
100	Yes (42)	Yes (40)	Yes (30)

Table 3 Simulation results for checking for which stress conditions the rock yield strength may be exceeded. Numerical values denote r at which the first time in the radial distance at which the tensile strength was exceeded.

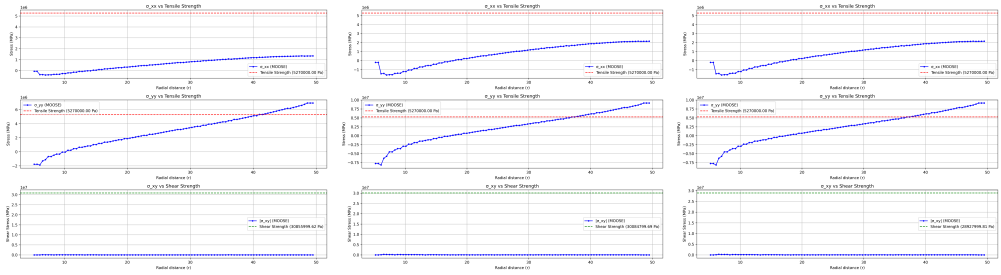

(a) $H = 100$ **(b)** $H = 80$ **(c)** $H = 50$

Figure 6 Simulations (Tensile) for one vertical fault in granite for the value of $K = 1$. Shear plots can be found at $\sim /2\_v\_fault/k1/d\_depth\_value$.

4.2.3 Comparison with Strength Criteria

- Granite's tensile strength: ~ 5.27 MPa
- Granite's shear strength: ~ 30 MPa

From Table3, we see that the tensile stresses most of the times exceed the strength. As the depth and K value increased the value of r at which this happened decreased i.e. failure near the tunnel. Shear stresses never really exceeded the shear strength for the angle values mentioned in section 4.2.1.

4.3 Interpretations

4.3.1 Physical Behavior

- Higher K (i.e., greater horizontal stress) increased shear stress on the fault interface.
- At $\theta = 0°$ and $\theta = 90°$ (along and perpendicular to the fault), stress concentration effects were more prominent.
- Modeling the contact with friction allowed for realistic slip and separation near the fault this closely mimiks the discontinuity behavior.

4.3.2 Accuracy and Error Analysis

- For the cases in coloumn 1 and 3 in the table3, we had to solve with decreases accuracy around 1e-5 since with a higher accuracy than that the linear and nonlinear solver were not converging. They converged at higher accuracy 1e-9 only for the $K = 1$ cases. We also decreased number of iterations to 200 (from the original 400) to ensure convergence.

4.3.3 Computational Cost and Stability

- For the given accuracy specified in section 4.3.2 above, the convergence was obtained within 1-2 minutes, otherwise it simply didnot converge since we restrcited the number of iterations.

5 Step3: Effect of Fault Orientation

For this part we study the impact of different fault orientations (other than the vertical fault orientation done in section 4)—**horizontal**, **45° inclined**, and **135° inclined**—on tunnel stability under varying in-situ stress ratios and depths. The focus is to identify the least favorable orientation for tunnel design, if tensile and shear yield stress have to be avoided.

5.1 Model Setup

- **Geometry:** A circular tunnel embedded in a rectangular domain (100×100 m), intersected by a single fault. The tunnel diameter remains consistent at 10 m. The fault is modeled as a discontinuity across the domain, oriented horizontally (0°), 45°, or 135°.

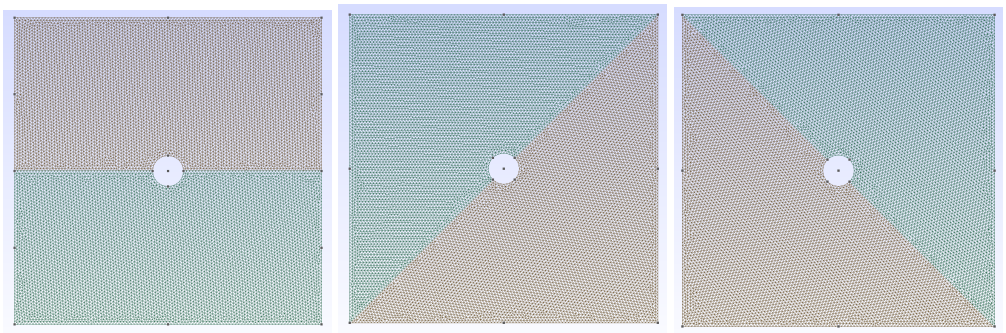

(a) Fault oriented at 0° **(b)** Fault oriented at 45° **(c)** Fault oriented at 135°

Figure 7 Meshes showing different fault orientations. Geometry created using gmsh and meshing done on the same.

- **Material, Constitutive Model, Fault Modeling Parameters, Boundary Conditions, Mesh and Interpolation, Solver Settings:** Same as the one used for vertical fault. We just write different .geo files for the three orientations, mesh them and pass to the MOOSE input file.

5.2 Results

For each fault orientation, we perform a full factorial design for three different values of p relating to depth and threee different values of K. This results in 9 experiments for each orientation and a total of 54 shear and tension results to compare the least favorable design.

- **Shear stress vs radial distance** from the tunnel center at angular positions $\theta = 0°, 15°, 30°, 45°, 60°, 90°$.
- **Stress components:** $\sigma_{xx}, \sigma_{yy}, \sigma_{xy}$ around the tunnel boundary.

- **Yield condition check:** The simulated stress magnitudes are compared with granite's tensile and shear strength values to determine the possibility of failure initiation.

Following tables indicate when does the streses exceed the tensile strength for axial streses. Shear stresses have remained below the yield points for all the cases.

Depth (m)	K = 0.5	K = 1.0	K = 1.5
50	No	No	No
100	No	No	No
200	No	Yes (42)	Yes (39)

Table 4 Simulation results (Horizontal Fault) for checking for which stress conditions the rock yield strength may be exceeded. Numerical values denote r at which the first time in the radial distance at which the tensile strength was exceeded.

Depth (m)	K = 0.5	K = 1.0	K = 1.5
50	Yes (48)	Yes (45)	Yes (45)
100	Yes (46)	Yes (45)	Yes (44)
200	Yes (45)	Yes (42)	Yes (8)

Table 5 Simulation results ($\theta = 45°$) for checking for which stress conditions the rock yield strength may be exceeded. Numerical values denote r at which the first time in the radial distance at which the tensile strength was exceeded.

Depth (m)	K = 0.5	K = 1.0	K = 1.5
50	No	No	No
100	No	Yes (45)	Yes (48) Shear
200	Yes (9)	Yes (38)	Yes (46) Shear

Table 6 Simulation results ($\theta = 135°$) for checking for which stress conditions the rock yield strength may be exceeded. Numerical values denote r at which the first time in the radial distance at it was exceeded.

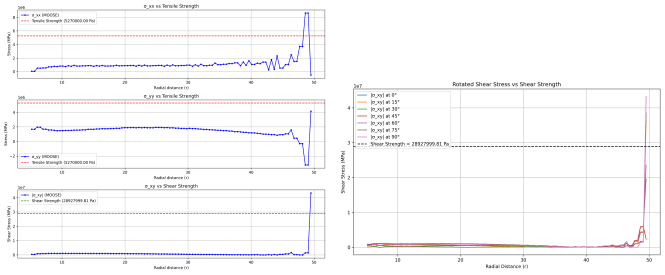

(a) Tensile Stress Evolution Radially

(b) Shear Stress Evolution Radially

Figure 8 Axial and Shear Stress evolution for fault oriented at ($\theta = 45°$).

5.3 Interpretations

We do the analysis at $(\theta = 45°, 135°, 90°, 0°)$. $\theta = 45°$ analysis is chosen so that we can observe the trend on how the analysis would change going from vertical to horizontal. Although a symmetric case to $\theta = 45°$, $\theta = 135°$ gives us the analysis on the negative radial direction for the $\theta = 45°$ case. Observations from simulations on different fault orientations are listed below:

- **Horizontal Fault:** Generally shows lower peak shear stress around the tunnel. The influence is more distributed. For higher K and depth, localized tensile zones may form on the crown and invert.
- **45° Fault:** This orientation produces the most *asymmetric* stress distribution, often concentrating shear stress along diagonal sections of the tunnel. This leads to high σ_{xy}, and the tunnel boundary near $\theta = 45°$ becomes critical for both shear and tensile failure.
- **135° Fault:** Displays behavior similar to 45°, but with stress concentrations mirrored across the vertical axis. This orientation also creates significant tensile and shear, particularly under oblique loading (higher K).
- **Shear Stresses:** Unlike seen previously, shear stresses in the $\theta = 45°$, surpass the yield strength near the domain boundary.
- **Most Critical Configuration:** The combination of $K = 1.5$ and depth = 200 m under the 45° fault orientation consistently led to maximum stress exceeding yield strength, especially at $\theta = 45°$ and $135°$. Tensile failure was more likely near the tunnel. In general from the table, vertical fault is also a very bad case as it induces failure not necessarily near the tunnel boundary but in almost all cases at some distance from the tunnel. The takeaway is that a lower K and a fault near the horizontal line would be the best case scenario.

- **Computation Cost and Accuracy:** Each simulation took approximately 2–4 minutes, longer than the previous simulations. Also, like the vertical fault case, we had to settle for lower accuracy (1e-5 compared to 1e-9) for other cases as the solver was not converging for higher depths for values $\neq$K=1.$We also decreases the number of iterations from 400 to 200 due to non-converging issues and this might also have stability issues in the solver.$

5.4 Conclusion

Among the four fault orientations studied, the **45° fault** and vertical fault under high K and depths pose the greatest risk of shear and tensile failure around the tunnel. In contrast, the **horizontal fault orientation** is a better preferred case for stress distribution and is relatively more favourable for tunnel design. This suggests that avoiding fault intersections at oblique angles can improve tunnel safety under non-isotropic stress fields.

6 Challenges, Limitations and Notes

1. We modeled the problem as a 2D case. But this makes sense since it is a plane strain case.
2. We were not able to visualize the output files through Paraview, the tool prescribed in the tutorial as it had issues loading files on macOS. No file processed beyond 40%. Therefore, we had to take an aletrnative approach to sample data and then read it through a python code, plot and do the analysis for failure.

3. For the cases with fault, we could not specify a different mesh refinement strategy near the tunnel, since even without that the solvers were not converging in many cases and we had to settle for lower accuray.
4. Not all the images and relevant data coudl be added to the report as online Latex software has a compile time limit and can not handle those many images. All the codes, plots, and data csv files can be retrieved and viewed at the github repository.

7 References

1. `https://www.engineeringtoolbox.com/young-modulus-d_417.html`
2. Study on the rock physical mechanical properties evaluation of tight oil reservoir in Chang 7 member, Longdong area, Ordos Basin, China.
3. `https://www.engineeringtoolbox.com/poissons-ratio-d_1224.html`
4. Hampton, J., Frash, L., Matzar, L., & Gutierrez, M. (2018). Extended-term monitoring of acoustic emissions post-laboratory hydraulic fracturing. ARMA US Rock Mechanics Symposium.
5. MOOSE-tuto-4-project1c.pdf (Canvas Tutorial from the course)
6. MOOSE-tuto-1.pdf (Canvas Tutorial from the course)
7. MOOSE-tuto-2-project1a.pdf (Canvas Tutorial from the course)